Strong Field Acceleration and Steering of Ultrafast Electron Pulses from a Sharp Metallic Nanotip

Doo Jae Park,[1,2] Bjoern Piglosiewicz,[1,2] Slawa Schmidt,[1,2] Heiko Kollmann,[1,2] Manfred Mascheck,[1,2] and Christoph Lienau[1,2,*]

[1]*Institut für Physik, Carl von Ossietzky Universität, 26129 Oldenburg, Germany*
[2]*Center of Interface Science, Carl von Ossietzky Universität, 26129 Oldenburg, Germany*

(Received 3 July 2012; published 11 December 2012)

We report a strong, laser-field induced modification of the propagation direction of ultrashort electron pulses emitted from nanometer-sized gold tapers. Angle-resolved kinetic energy spectra of electrons emitted from such tips are recorded using ultrafast near-infrared light pulses of variable wavelength and intensity for excitation. For sufficiently long wavelengths, we observe a pronounced strong-field acceleration of electrons within the field gradient at the taper apex. We find a distinct narrowing of the emission cone angle of the fastest electrons. We ascribe this to the field-induced steering of subcycle electrons as opposed to the diverging emission of quiver electrons. Our findings are corroborated by simulations based on a modified Simpleman model incorporating the curved, vectorial field gradient in the vicinity of the tip. Our results indicate new pathways for designing highly directional nanometer-sized ultrafast electron sources.

DOI: 10.1103/PhysRevLett.109.244803 PACS numbers: 41.75.Jv, 34.50.Fa, 79.60.Jv, 79.70.+q

In atomic and molecular systems, the interaction of electrons with strong laser fields approaching or exceeding the interatomic field strength gives rise to a wealth of interesting phenomena, including high harmonic generation [1–3], attosecond streaking [4–7], or the generation of attosecond electron wave packets for tomographic imaging of molecular orbitals [8]. Quite recently, the first observations of strong-field phenomena in the interaction of light with solid state nanostructures have been reported, including ponderomotive acceleration and carrier-envelope phase effects in photoemission from metallic surfaces [9,10] and dielectric nanospheres [11], or high harmonic generation from plasmonic nanoantennas [12,13]. In particular, sharp nanometer-sized metallic tips are emerging as a test bed for exploring various strong-field phenomena, revealing, for instance, multiphoton ionization (MPI) [14,15], above threshold ionization (ATI) [16], and optical field emission [17,18] regimes.

Strong-field photoemission from such metallic nanostructures differs substantially from that in atomic and molecular systems. Specifically, the large optical field enhancement $f \approx 10$ at the very apex of gold tapers [15,17] greatly reduces the laser intensities needed to reach the strong-field regime and thus alleviates the need for high-power, low-repetition rate lasers. In addition, the decay length of the associated evanescent field is as short as a few nanometers only, resulting in strong gradients of the acceleration field seen by the photo-emitted electrons. This can suppress the quiver motion of the electrons within the oscillating electric field [19] once the near-field decay length l_F becomes shorter than the quiver amplitude $l_q = efE_0/(m\omega^2)$, where E_0 the denotes the field amplitude at frequency ω, e the charge, and m the mass of the electron. These field gradients may not only affect the kinetic energy but also the emission direction, i.e., the path of the photoejected electrons, potentially paving the way towards highly directional electron sources with femtosecond time resolution [17,18,20]. So far, however, little is known about light-driven modifications of electron pathways from such nanometer-sized tips. Previous experiments revealed emission cone angles of more than 30°, reduced by only a few percent when crossing the transition from multiphoton to strong-field emission [17].

In this Letter, we study angle-resolved kinetic energy spectra of electrons emitted from sharp gold tips illuminated with intense ultrashort near-infrared (NIR) light pulses of variable wavelength and intensity. For sufficiently long laser wavelengths, we observe a distinct narrowing of the emission cone angle and hence a laser-induced steering of the electron motion. Our results are corroborated by a quasiclassical model for the electron motion incorporating the vectorial field gradient at the apex. These simulations suggest that this light-driven modification of the electron path is most efficient for those electrons that traverse the field gradient within less than half an optical cycle.

Photoelectrons are generated by focusing ultrashort NIR laser pulses onto sharp metallic tips [experimental setup in Fig. 1(a)]. The NIR pulses are generated in a noncollinear optical parameteric amplifier delivering ~30-fs pulses with a center wavelength tunable between 1.0 and 1.5 μm and with a nonstabilized carrier-envelope phase. The metal tip is a sharply etched, single-crystalline gold taper [Fig. 1(b)] mounted inside a vacuum chamber. A new fabrication method described in Ref. [21] generates tips with an extremely small apex radius of around 7 nm.

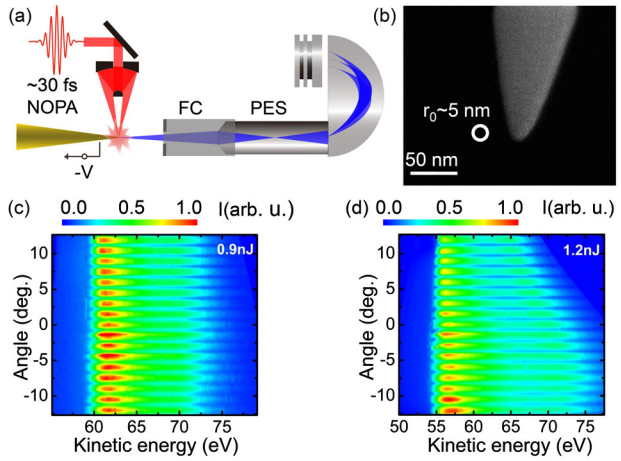

FIG. 1 (color online). (a) Experimental setup. Ultrashort laser pulses with ~30-fs duration are focused onto a sharp gold tip with $r_0 \sim 5$ nm (b) inside a vacuum chamber. Angle-resolved kinetic energy spectra $I(E_{\mathrm{kin}}, \theta)$ are recorded using a PES, a Faraday cage (FC) minimizes static field distortions. (c) Spectrum $I(E_{\mathrm{kin}}, \theta)$ recorded for 1.5 μm center wavelength and 0.9 nJ pulse energy showing that electrons are emitted into a broad angle. (d) Spectrum $I(E_{\mathrm{kin}}, \theta)$ recorded at higher pulse energy of 1.2 nJ revealing a clear narrowing of the emission angle for the largest kinetic energies.

To avoid pulse dispersion, all-reflective optics are applied and a Cassegrain objective is used to achieve tight focusing to <1.5 μm [22]. The incident pulse energy is varied from 0.08 to 1.2 nJ, corresponding to peak intensities ranging from $\sim 10^{11}$ to $\sim 1.8 \times 10^{12}$ W/cm^2 and to Keldysh parameters $\gamma = \omega\sqrt{2m\Phi}/(ef E_0)$ between 1.5 and 0.3 when taking a field enhancement factor $f \approx 10$ [15] and a work function Φ of 5.5 eV, thus crossing the transition from multiphoton to optical field emission [17]. Angle-resolved kinetic energy spectra are recorded with a hemispherical photoelectronspectrometer (PES) equipped with a two-dimensional CCD detector. A Faraday cage (FC) is used to minimize static field distortions induced by nearby objects, i.e., the Cassegrain objective and sample translation stages. A transmission grating consisting of equally separated metallic wires in front of the FC allows for a precise measurement and correction of faint residual variations of the emission angle ($<0.05°$/eV) using their shadow image when recording angle-resolved kinetic energy spectra at low laser pulse energy. This setup provides an energy resolution of ~0.2 eV and an angular resolution of ~0.1°.

Angle-resolved energy spectra $I(E_{\mathrm{kin}}, \theta)$ obtained by illuminating gold tips with 30-fs pulses of 1.5 μm center wavelength and with pulse energies of 0.9 and 1.2 nJ are displayed in Figs. 1(c) and 1(d), respectively. Here, a small negative dc bias of $U_B \sim 50$ eV [in (c)] and ~45 eV [in (d)] is applied to the tip to avoid static charging and undesired charged particle attachments during electron emission. The horizontal dark stripes are the shadows of the aforementioned metallic transmission grating in front of the Faraday cage. Two distinct features can be observed in Figs. 1(c) and 1(d). First, the kinetic energy distribution of the photoelectrons extends over broad ranges of ~12 eV for 0.9 nJ and ~20 eV for 1.2 nJ pulse energy. This is the signature of strong-field acceleration within the near field of the tip. The second and important observation is a qualitative difference in angular distribution: At 0.9 nJ pulse energy, the electrons are homogeneously distributed over a broad emission angle, whereas at 1.2 nJ we observe a narrowing of the emission cone angle, which becomes more pronounced as the kinetic energy increases. This latter observation is a clear indication for a laser-driven modification of the emission direction of the strong-field accelerated electrons.

To understand the microscopic origin of this steering phenomenon, we have recorded power-dependent angle-integrated spectra $\bar{I}(E_{\mathrm{kin}})$ with a negative dc bias of $U_B \sim 90$ eV for different laser wavelengths. Figure 2(a) displays spectra at 1 μm and with pulse energies between 0.12 and 0.6 nJ. At low powers, we see a narrow emission spectrum characteristic for MPI. Its width is given by a convolution of electron temperature, laser spectral bandwidth, and spectrometer resolution. When increasing the pulse energy, its shape becomes broader, showing a more gradual exponential decay on the high-energy side, presumably reflecting the increase in electron temperature during the optical excitation [15] and the onset of ATI [23]. At the highest

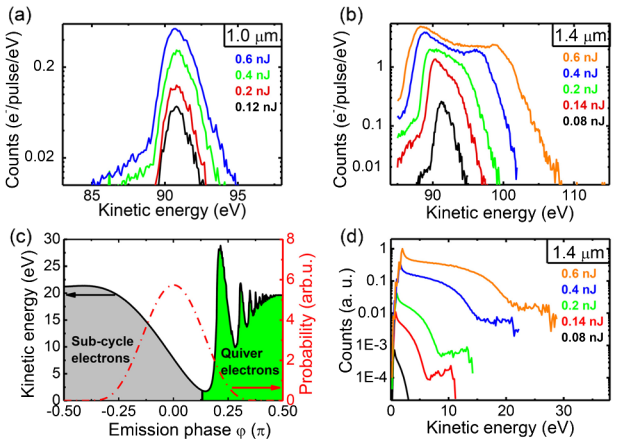

FIG. 2 (color online). (a, b) Angle-integrated spectra for different incident pulse energies, measured with excitation center wavelengths of 1.0 and 1.4 μm. In (a), the pulse energy varies from 0.12 nJ (bottom) to 0.6 nJ (top) and in (b) the pulse energy varies from 0.08 nJ (bottom) to 0.6 nJ (top). (c) Calculated terminal kinetic energy distribution (black solid curve) and electron generation probability (red dash-dotted curve) as a function of emission phase. The simulations are performed for 30 fs pulse duration, 1.4 μm center wavelength, and 25.4 V/nm peak electric field strength (near field decay length of 1.5 nm). (d) Simulated kinetic energy spectra for laser pulse energies from 0.08 (black curve at the bottom) to 0.6 nJ (orange curve at the top) with a fixed wavelength of 1.4 μm.

pulse energy, we see a weak exponential tail at low E_{kin}, most likely a first indication of a laser-induced reduction of the tunneling barrier. These spectra show little evidence for laser-induced electron acceleration, in agreement with predicted Keldysh parameters $\gamma > 0.6$. At such short wavelengths lower γ values are prohibited by thermal tip damage. This scenario changes drastically when increasing the excitation wavelength to 1.4 μm [Fig 2(b)]. While low-intensity kinetic energy spectra are again governed by MPI and ATI, much broader plateaulike spectra are revealed for pulse energies >0.1 nJ. The plateau region expands towards both sides until the width of the plateau exceeds 20 eV at 0.6 nJ. Compared to spectra known from high harmonic generation [1,24,25], the relative intensity of the plateau with respect to the peak at U_B is much more pronounced. Such plateaulike spectra have recently been observed for midinfrared wavelengths [19] and have been attributed to strong-field acceleration of electrons within the steep near-field gradient at the tip apex. Here, we observe such spectra for the first time for much shorter NIR wavelengths.

To account for these spectral shapes, we have performed numerical simulations of electron trajectories within an extended semiclassical Simpleman model [26]. We assume a two-dimensional hyberboloidal gold tip with an opening angle of $\alpha = 30°$ and use existing analytical expressions to describe the tip's near-field $\vec{E}(\vec{r}, t)$ [27]. We model the time structure of the field as a cosine carrier wave with frequency ω, fixed carrier-envelope phase, $\phi_{\mathrm{CEP}} = 0$, and an envelope matching the experimental pulse duration. A Fowler-Nordheim equation [28] neglecting field-dependent barrier suppression and assuming electron generation only during negative half-cycles (electron acceleration away from the tip) describes the tunneling probability as a function of the birth time $t = \varphi/\omega$ of the electron (φ: emission phase). Electron motion is simulated under the action of the force field $\vec{F}(\vec{r}, t) = q \cdot \vec{E}(\vec{r}, t)$, treating recollisions with the tip as perfect elastic collisions with a yield of unity [16]. Kinetic energy spectra are generated by averaging over a distribution of emission phases and sites. Such a model has recently successfully been used to describe different strong-field photoemission phenomena [16,19] and has been tested against different more refined approaches [29]. Within this model, the shape of the spectrum, in particular the amplitude and formation of the plateau region, depends sensitively on both the pondermotive potential $U_P = (efE_0)^2/(4m\omega^2)$ and the decay length l_f, with a high-energy cutoff decreasing with decreasing l_f and U_p [19]. Figure 2(c) illustrates the kinetic energy distribution and the corresponding generation probability of electrons calculated as a function of the emission phase for an incident laser wavelength of 1.4 μm. We find that the shape of the energy spectrum, specifically the plateau region, depends sensitively on the decay length l_f. To approximate the spectrum in Fig. 2(b), a rather small value of $l_f = 1.5$ nm and a field enhancement $f = 9$ is needed. The absolute value of l_f is sensitive to the tip geometry and slightly different values might be deduced for nonhyperboloidal shapes. This results in a near-field amplitude $fE_0 = 25.4$ V/nm (at 0.6 nJ) and a quiver amplitude of $l_q = 2.4$ nm, which is substantially larger than l_f. We thus estimate an adiabaticity parameter of $\delta = l_f/l_q = 0.63$, indicating that these spectra probe electron dynamics in the subcycle regime [19]. Under these conditions, most of the electrons that leave the tip, namely those emitted for $\phi < 0.12\pi$, escape from the near-field zone within less than one optical cycle and directly traverse the short near-field gradient, resulting in a smooth, plateaulike kinetic energy distribution [gray shaded area in Fig. 2(c)]. Only the remaining electrons ($\phi \geq 0.12\pi$) are in the traditional quiver regime. As a consequence, the kinetic energy minimum is shifted away from the maximum generation probability at $\phi = 0$, suppressing the strong low energy peak and enhancing the high-energy plateau region. As expected from $l_q \propto fE_0$, for higher pulse energies the plateau formation is progressively enhanced [Fig. 2(d)], in good qualitative agreement with the experiment. For the chosen pulse duration, the calculated spectra are essentially independent of φ_{CEP}, whereas a phase-dependent cutoff energy is expected for much shorter pulses.

With this insight we can discern the contribution of two emission mechanisms in Figs. 1(c) and 1(d): Cross sections shown in Fig. 3(a) indicate that at all angles the spectra are well described as a superposition of an exponential decay ($e^{-(E-E_0)/\Delta E}$) representing MPI and ATI electrons and a plateaulike section at the higher energies reflecting strongly accelerated subcycle electrons, which can be approximated by a Gaussian distribution. Both at low and high pulse energies, the decay energy ΔE is independent of the emission angle, indicating that the laser field hardly affects the directionality of MPI electrons, resulting in a broad emission cone angle exceeding 30° [17]. The angle dependence of the residual Gaussian contribution is depicted in Figs. 3(b) and 3(c). At low pulse energy, we observe negligible angle variation [Fig. 3(d)]. Apparently, the kinetic energy gained during the acceleration process is not yet sufficient to markedly alter the path of the electrons.

In contrast, spectra acquired at a higher pulse energy of 1.2 nJ [Fig. 3(c)] display a distinct dependence of both maxima and high energy cutoff of the energy distribution on the emission angle. A maximum high energy cutoff is seen for an emission angle of −8°, possibly reflecting a slight tilt of the tip with respect to the spectrometer. The maximum of the kinetic energy decreases both towards larger and smaller angles by about 0.4 eV/degree. Clearly, the emission cone angle is substantially reduced for the fastest electrons down to ~12° at $E_{\mathrm{kin}} = 75$ eV [Fig. 3(e)], as compared to a cone angle of >30° for the quiver electrons [17].

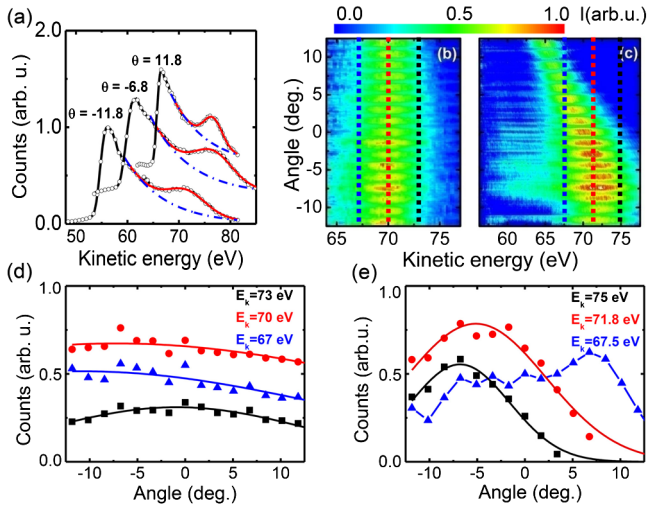

FIG. 3 (color online). (a) Spectra for three different detection angles of $\theta = -11.8°$, $-6.8°$, and $11.8°$ (black curves), replotted from Fig. 1(d). The data are well approximated by the superposition (red solid lines) of an exponential decaying part (blue dash-dotted lines) and a Gaussian distribution of strongly accelerated electrons. Angle-dependent kinetic energy spectra $I(E_{\mathrm{kin}}, \theta)$ of the strongly accelerated electron distribution for pulse energies (b) of 0.9 and (c) of 1.2 nJ. (d) Cross sections through (b) at fixed E_{kin} of 73 (black squares), 70 (red circles), and 67 eV (blue triangles), obtained by averaging the data over 1.7° and 0.15 eV; solid lines are to guide the eye. (e) Cross sections through (c) at $E_{\mathrm{kin}} = 75$ (black squares), 71.8 (red circles), and 67.5 eV (blue triangles) together with Gaussian-shaped fits for 71.8 and 75 eV.

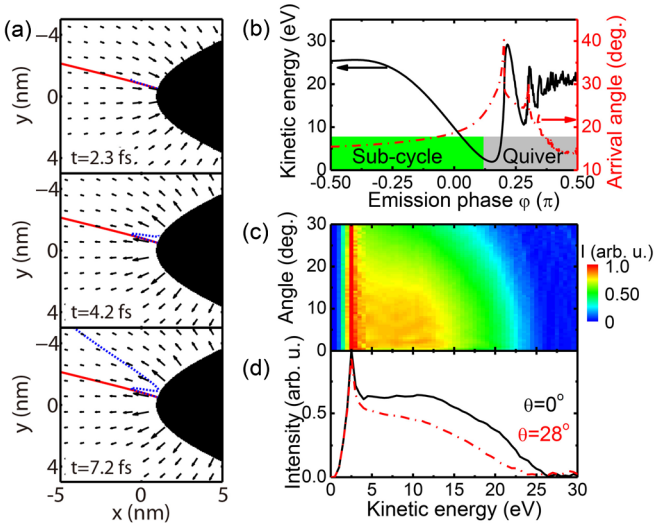

FIG. 4 (color online). (a) Snapshots of two representative simulated electron trajectories for subcycle electrons ($E_{\mathrm{kin}} = 25$ eV, red solid line) and quiver electrons (3.5 eV, blue dotted line) at times 2.3, 4.2, and 7.2 fs after the birth of the electrons at an emission site $y = 0.5$ nm offset from the tip axis illuminated with 1.5 μm wavelength and $fE_0 = 28.0$ V/nm peak electric field strength ($l_f = 1.5$ nm). The vectorial electric field distribution in the vicinity of the tip apex (black solid) is indicated by black arrows. (b) Calculated terminal kinetic energy E_{kin} (black solid curve) and angle of arrival θ_∞ (red dash-dotted curve) as a function of emission phase ϕ for electrons from the same emission site as (a). (c) Angle-dependent kinetic energy spectrum $I(E_{\mathrm{kin}}, \theta_\infty)$ calculated by averaging electrons emitted at different phases and sites. (d) Cross section through (c) for $\theta_\infty = 0°$ (black solid curve) and $\theta_\infty = 28°$ (red dash-dotted curve).

These findings are reasonably well understood in terms of the two-dimensional Simpleman model introduced above. Figure 4(a) depicts snapshots of two representative electron trajectories in the subcycle regime ($\varphi = -\pi/2$, $E_{\mathrm{kin}} = 25$ eV, red line) and in the quiver regime ($\varphi = 0.18$, $E_{\mathrm{kin}} = 3.5$ eV, blue line), respectively, generated 0.5 nm off the tip center with 1.5 μm laser wavelength and $fE_0 = 28.0$ V/nm. Initially, both electrons are accelerated along the direction of the field lines at the tip surface ($\Delta t = 2.3$ fs). The subcycle electrons are accelerated out of the strong near field during the first half-cycle, such that their ponderomotive energy is gained during this initial half-cycle acceleration period and hence their trajectories are only weakly affected by subsequent laser field oscillations. The quiver electrons, however, cannot escape from the near-field region within such a short time. They experience a strong back acceleration within the second half-cycle and undergo a complicated quiver motion, potentially recolliding with the tip surface. Local magnetic fields are weak and play only a minor role for the electron motion. The pronounced field guiding effect is illustrated in Fig. 4(b) by plotting the terminal emission angle $\theta_\infty = \theta(t \to \infty)$ as a function of emission phase ϕ for the same emission spot as Fig. 4(a). While the fastest subcycle electrons ($\varphi < -0.25\pi$) are ejected along the surface normal ($\theta = 15°$), the arrival angle increases greatly to $\theta_\infty > 30°$ for quiver electrons ($\varphi > 0.12\pi$). A simulated angle-resolved kinetic energy spectrum obtained by integrating over a range of emission sites [Fig. 4(c)] shows the same qualitative behavior as the experimental measurements [compare Fig. 1(d)]. The simulations indicate that for short, near-ir wavelengths, strong-field steering of electrons occurs in the vicinity of nanostructures with large local field enhancement and steep field gradients. For longer wavelength and correspondingly larger quiver amplitude, similar phenomena are also anticipated in geometrically less confined nanostructures.

In conclusion, we have reported the first angle-dependent kinetic energy spectra of strong-field accelerated electrons photoemitted from sharp, nanometer-sized gold tips, observing a distinct narrowing of the emission cone angle of the fastest electrons. Our results, qualitatively described by a modified two-dimensional semiclassical model for the electron generation and acceleration, suggest that the strong electric field gradients in the vicinity of such metallic nano-objects not only define the kinetic energy but also the direction of the electron movement, allowing for guiding electrons along optical field line

gradients. Such near-field steering of electrons could be of interest, e.g., for temporally and/or spatially gating electron pulses by strong surface plasmon polariton fields, potentially allowing for probing the motion of electrons in nanostructures with high temporal and spatial resolution.

Financial support of the work by the Deutsche Forschungsgemeinschaft (SPP1391), by the European Union (''CRONOS''), and the Korea Foundation for International Cooperation of Science and Technology (Global Research Laboratory project, K20815000003) is gratefully acknowledged. D. J. P. wishes to thank the Hanse-Wissenschaftskolleg for support. The authors would like to thank P. Gross and P. Schreip for valuable discussions. D. J. P., B. P., and S. S. contributed equally to this work.

*Corresponding author.
christoph.lienau@uni-oldenburg.de

[1] P. B. Corkum, Phys. Rev. Lett. **71**, 1994 (1993).
[2] G. G. Paulus, F. Grasbon, H. Walther, P. Villoresi, M. Nisoli, S. Stagira, E. Priori, and S. De Silvestri, Nature (London) **414**, 182 (2001).
[3] J. L. Krause, K. J. Schafer, and K. C. Kulander, Phys. Rev. Lett. **68**, 3535 (1992).
[4] P. Eckle, M. Smolarski, P. Schlup, J. Biegert, A. Staudte, M. Schöffler, H. G. Muller, R. Dörner, and U. Keller, Nat. Phys. **4**, 565 (2008).
[5] G. G. Paulus, F. Lindner, H. Walther, A. Baltuška, E. Goulielmakis, M. Lezius, and F. Krausz, Phys. Rev. Lett. **91**, 253004 (2003).
[6] J. Itatani, F. Quéré, G. Yudin, M. Ivanov, F. Krausz, and P. Corkum, Phys. Rev. Lett. **88**, 173903 (2002).
[7] E. Goulielmakis, V. S. Yakovlev, A. L. Cavalieri, M. Uiberacker, V. Pervak, A. Apolonski, R. Kienberger, U. Kleineberg, and F. Krausz, Science **317**, 769 (2007).
[8] J. Itatani, J. Levesque, D. Zeidler, H. Niikura, H. Pépin, J. C. Kieffer, P. B. Corkum, and D. M. Villeneuve, Nature (London) **432**, 867 (2004).
[9] J. Kupersztych, P. Monchicourt, and M. Raynaud, Phys. Rev. Lett. **86**, 5180 (2001).
[10] A. Apolonski *et al.*, Phys. Rev. Lett. **92**, 073902 (2004).
[11] S. Zherebtsov *et al.*, Nat. Phys. **7**, 656 (2011).
[12] S. Kim, J. Jin, Y.-J. Kim, I.-Y. Park, Y. Kim, and S.-W. Kim, Nature (London) **453**, 757 (2008).
[13] M. Sivis, M. Duwe, B. Abel, and C. Ropers, Nature (London) **485**, E1 (2012).
[14] P. Hommelhoff, C. Kealhofer, and M. A. Kasevich, Phys. Rev. Lett. **97**, 247402 (2006).
[15] C. Ropers, D. R. Solli, C. P. Schulz, C. Lienau, and T. Elsaesser, Phys. Rev. Lett. **98**, 043907 (2007).
[16] M. Krüger, M. Schenk, and P. Hommelhoff, Nature (London) **475**, 78 (2011).
[17] R. Bormann, M. Gulde, A. Weismann, S. V. Yalunin, and C. Ropers, Phys. Rev. Lett. **105**, 147601 (2010).
[18] P. Hommelhoff, Y. Sortais, A. Aghajani-Talesh, and M. A. Kasevich, Phys. Rev. Lett. **96**, 077401 (2006).
[19] G. Herink, D. R. Solli, M. Gulde, and C. Ropers, Nature (London) **483**, 190 (2012).
[20] P. Dombi and P. Rácz, Opt. Express **16**, 2887 (2008).
[21] S. Schmidt, B. Piglosiewicz, D. Sadiq, J. Shirdel, J. S. Lee, P. Vasa, N. Park, D.-S. Kim, and C. Lienau, ACS Nano **6**, 6040 (2012).
[22] B. Piglosiewicz, D. Sadiq, M. Mascheck, S. Schmidt, M. Silies, P. Vasa, and C. Lienau, Opt. Express **19**, 14451 (2011).
[23] M. Schenk, M. Krüger, and P. Hommelhoff, Phys. Rev. Lett. **105**, 257601 (2010).
[24] G. G. Paulus, F. Grasbon, H. Walther, R. Kopold, and W. Becker, Phys. Rev. A **64**, 021401 (2001).
[25] M. Lewenstein, P. Balcou, M. Y. Ivanov, A. L'Huillier, and P. B. Corkum, Phys. Rev. A **49**, 2117 (1994).
[26] See Supplemental Material athttp://link.aps.org/supplemental/10.1103/PhysRevLett.109.244803 for a description of the model simulations.
[27] N. Behr and M. B. Raschke, J. Phys. Chem. C **112**, 3766 (2008).
[28] E. L. Murphy and R. H. Good, Jr., Phys. Rev. **102**, 1464 (1956).
[29] S. V. Yalunin, M. Gulde, and C. Ropers, Phys. Rev. B **84**, 195426 (2011).